Journal of Applied Fluid Mechanics, Vol. 18, No. 1, pp. 145-158, 2025.
Available online at www.jafmonline.net, ISSN 1735-3572, EISSN 1735-3645.
https://doi.org/10.47176/jafm.18.1.2772

Experimental Investigation of Active Microfluidic Cooling Solution to Processor Chip

D. S. Rawat[1†], M. S. Lodhi[2] and T. Sheorey[1]

[1] *Department of Mechanical Engineering, PDPM IIITDM Jabalpur-482005, Madhya Pradesh, India*
[2] *Department of Mechanical Engineering, SGSITS Indore-452003, Madhya Pradesh, India*

†*Corresponding Author Email: 1913801@iiitdmj.ac.in*

ABSTRACT

Heat sinks with microchannels were being studied as a viable thermal management option for electronic equipment. The total heat transfer characteristics of a microchannel heat sink are revealed based on fluid flow characteristics inside the microchannels along with convective heat transfer, both of which are controlled by channel design and flow configuration. The aim of the present investigation was to test the microchannel heat sink with Z-type flow configuration, using nanofluid as a promising solution to chip cooling technology. Experimental investigations were carried out to assess the impact of varying nanoparticle concentrations of Al_2O_3 with water as the base fluid on heat transfer and fluid flow performance on effective heat flux removal. The heat spreader of the Intel® Core™ i7 microprocessor chip was used as the microchannel test section, after separating it from the chip. A microchannel heat sink was then fabricated by cutting inlet and outlet ports and manifolds with ten parallel microchannels. Cartridge heaters were used to provide a thermal load with a constant heat flux of $95W/cm^2$, equivalent to the thermal design power of the actual processor chip. For the safe operation of the processor chip against performance degradation, experiments were conducted with varied Reynolds numbers in the range $1000 \leq Re \leq 1800$ to achieve the maximum temperature of the heat sink below the critical limit. Thermal IR imaging has been carried out to assess the temperature field. The Nusselt number and convective heat transfer coefficient exhibit a favourable improvement upon the addition of nanoparticles of about 25%, a clear benefit of having hydrodynamically and thermally developing flow fields. Finally, the Nusselt number and friction factor correlations were proposed. The accuracy of the developed correlations for the average Nusselt number and friction factor were within ±10% and ±8%, respectively. The presented research provides in-depth knowledge about the capability of Z-type microchannel heat sink with multi-microchannels for electronic processor chip cooling and its consequences for conditioning monitoring of forthcoming electronic gadgets.

Article History

Received April 7, 2024
Revised June 10, 2024
Accepted July 26, 2024
Available online November 6, 2024

Keywords:

Microchannel heat sink
Nanofluid
Z type parallel flow
Heat transfer
Nusselt number
Reynolds number

1. INTRODUCTION

Electronic integrated devices are essential in the present era of modernity. Electronic packaging like super computers, mobile phones, and mini-tab are becoming highly miniaturized with very large integration of semiconductors on a single chip. But the large-scale integration leads to generation of higher heat flux. The generated high heat flux should be essentially dissipated to the atmosphere for the safe operation of the devices. The microchannel heat sink (MCHS) with appropriate coolant and flow conditions may be feasible solution to cool the processor chip. It is the fundamental element of a microfluidic circuit that is widely used to cool electrical equipment like PV cells, pipeline networks, catalytic processors, and self-propelled regenerators. Research by many industries as well as academicians are underway to overcome the challenges in MCHS for dissipating higher heat flux and maintaining chip surface temperature below the critical limit. Researchers were working hard in the beginning of the 1980s to find a workable way to dissipate increased heat flux production from smaller chip surface areas (Tuckerman & Pease, 1981). The work led the way and pioneered the technique of microchannels (a substantial ratio of area covered to volume) for effectively eliminating elevated heat flux

NOMENCLATURE

A	area of microchannel	T_i	inlet temperature
c_p	specific heat capacity	T_m	mean fluid temperature
D_h	hydraulic diameter	T_o	outlet temperature
f	friction factor	T_s	surface surface temperature
h	heat transfer coefficient	V	volumetric flow rate
k	thermal conductivity	W	width of microchannels
L	length of microchannels	μ	dynamic viscosity
$\dot{m}$	mass flow rate	ρ	density
N	total number of microchannels	Nu	Nusselt number
p	pressure	Re	Reynolds number
Q	heat transfer rate	Pr	Prandtl number
q''	wall heat flux		

from tiny spaces. Subsequently, numerous experiments were conducted to enhance heat dissipation. Several investigators conducted scientific experiments throughout early phases of growth. However, outcomes for the friction factor with non-uniform fluid flow remained conflicting (Peng & Peterson, 1996; Herwig, 2002; Kandlikar & Grande, 2003; Kumaraguruparan et al., 2011). Subsequently, other investigators submitted their findings on one-channel, single phase fluid circulation and discovered an excellent match between the experimental and numerical data for friction factor (Xu et al., 2000; Morini, 2004; Vijayalakshmi et al., 2009). Various researches have thoroughly investigated the problems encountered in MCHS for the enhanced heat transfer and fluid flow and recommendations have been made for geometrical modification in channels as well as manifold and inlet outlet ports, shape and sizes (Rostami et al., 2002; Roday & Jensen, 2009; Chai et al., 2013; Mohammed Adham et al., 2013; Smakulski & Pietrowicz, 2016; Datta et al., 2019; Alihosseini et al., 2020; Ramesh et al., 2021). Peyghambarzadeh et al. have performed an experimental investigation in a rectangular microchannel heat sink to observe the impact of Re numbers (500 to 2000) and nanofluids (Al_2O_3/water and CuO/water) using particle concentrations (0-1vol.%) on heat transfer and flow fields. They considered the MCHS having 17 microchannels at fixed heat flux ($190\,kW/m^2$). Using Al_2O_3/water and CuO/water nanofluid, they reported 27.2% and 49.01% enhancement respectively in the average value of heat transfer coefficient (HTC) over distilled water (DW) (Peyghambarzadeh et al., 2014). Chabi et al. performed the experimental study on fluid flow and heat transfer characteristics in multi-MCHS having 17 microchannels ($W = 400\mu m\ and\ H = 560\mu m$) with CuO/water nanofluid (1 and 2 vol.%) and Reynolds numbers (600 to 1800). The finding obtained was more than 40% increment in average HTC at Reynolds number of 1150 with 0.2 vol.% of nanofluid particle concentration then that of the DW (Chabi et al., 2017). In another experimental investigation, Bowers et al. examine the heat transfer characteristics influenced by the Al_2O_3/water and SiO_2/water nanofluids (1 and 2 vol.%) in a rectangular MCHS (N=5, $L = 58mm$, and W=60-300mm). They observed that the microchannels with the width of 180mm and 300mm provided maximum enhancement in heat transfer about 40% and 20% respectively over the DW (Bowers et al., 2018). Nikkhan et al. experimentally investigated with varied heat fluxes (10 kW/m^2 to 70 kW/m^2) using MCHS having multi microchannels and ZrO_2/water nanofluid of 0.1- 0.3 wt.% particle concentration. Results indicated that the nanofluid with 0.3wt.% provides better heat transfer rate about 13.9% over the DW. They also computed the friction factor and reported enhancement about 17.3% (Nikkhah & Nakhjavani, 2019). Some researchers experimentally investigated the MCHS in order to improve the capability of heat removal rate and subsequent correlation development for nanofluid using cylindrical MCHS with multi microchannels using variable heat flux (35 and 50 kW/m^2) at Reynolds numbers (200 to 900) (Azizi et al., 2015, 2016). They considered the MCHS dimensions as D_h =526 mm, L=50mm and N =86. They concluded that the use of Cu/water nanofluid (0.3wt.%) provided better enhancement in Nusselt number about 43% and friction factor of about 45.6% over the DW. They also concluded that the average Nusselt number and friction factor correlations provide a better comparison with the accuracy of ±10 % using experimental data. Manay and Sahin had also performed experimental investigation to observe the microchannel height influence for increased heat transfer removal rate and uniformed flow conditions in MCHS. They also developed correlation using TiO_2/water nanofluid (0.25-2 vol.%). They considered MCHS with flow Reynolds numbers in the range of 50 to 750 and constant heat flux($80kW/m^2$) at the bottom wall. From the experiment, it was found that a 200mm channel height provides an enhanced value of average HTC and friction factor of 46% and 20%, respectively, with nanofluid. They also showed that the data obtained from correlations and experimental investigation for average Nusselt number and friction factor agreed well (Manay & Sahin, 2016a, 2017). Behi et al. also performed experimental investigation using circular microchannel (L= 30cm length and 0.50mm internal diameter was examined by using Al_2O_3/water nanofluid along with the particle concentration (1 to 5.5vol.%), size of nanoparticle ranging from 13 to 130 μm and Reynolds number (400 to 2180). From the investigation they concluded that the 42.1% and 22.3% increment in Nusselt number and friction factor respectively was observed at 5.5 vol.% of nanoparticle concentration. They also put forward the correlations for Nusselt number and friction factor for alumina nanofluid in DW that provide reasonable variations in the comparison of

experimental and proposed correlation data (Behi et al., 2020).

Several investigators were working to improve the heat transmission capabilities and flow characteristics in MCHS. The flow arrangement, type of coolant and Reynolds number, all together contribute to the thermal performance of MCHS. Different nanofluids $(Al_2O_3, CuO, SiO_2, TiO_2)$ with different nanoparticle concentration in base fluid (water, EG, and coolants) are the key factors that affect the thermal transport phenomena in MCHS. Researchers were looking at how different flow paths affect the thermal efficiency of MCHS. But no comprehensive empirical investigation had been published to date to comprehend the impact of heat transfer inside the MCHS with Z-type flow configuration and $Al_2O_3/water$ nanofluid at different nanoparticle concentrations as coolant for industry grade processor chip cooling.

The motive of current investigation was to examine the MCHS as a possible solution to cool the processor chip in actual industrial application. Further, the experimental study on fluid flow and heat transfer analysis with the Z-type flow configured MCHS using varying concentrations of $Al_2O_3/water$ nanofluid as a coolant was carried out. The Reynolds number was varied to enhance the convective heat transfer in order to keep the highest surface temperature of the MCHS below its critical limit. The temperature of MCHS channel wall surface was measured in the form of thermo-graphic imaging captured by thermal IR camera. Moreover, the correlations of Nusselt number and friction factor were also developed. The presented research provides an elaborate study on the capability of multi-microchannel Z-type configured MCHS for the cooling of electronic processor chip.

2. EXPERIMENTAL SETUP AND WORKING FLUID

2.1 MCHS Design and Fabrication

The laboratory arrangement was designed and developed to investigate the thermal and fluid flow features of $Al_2O_3/water$ nanofluid in Z-type parallel flow multi-microchannel heat sink. In view of the industrial application of microchannel heat sink for cooling of electronic processor chip, an actual heat spreader $(30mm \times 30mm)$ of Intel® Core™ i7 CPU was used as shown in Fig.1(a). The processor chip was carefully removed from the heat spreader. The optimized design parameters obtained from simulation were considered to fabricate the MCHS with Z-type flow arrangement (Fig. 1(b)). Ten square microchannel $(500\mu m \times 500\mu m)$ having the length of 10mm, inlet/outlet ports $(830\mu m \times 830\mu m)$ having length of 8 mm and inlet/outlet manifolds $(11mm \times 3mm \times 750\mu m)$ were cut using micro grain carbide end mill cutter $(D_{Tip} = 500\mu m, D_{shank} = 4mm \; and \; L = 50mm)$ in CNC milling machine available at institute advance machining centre.

(a)

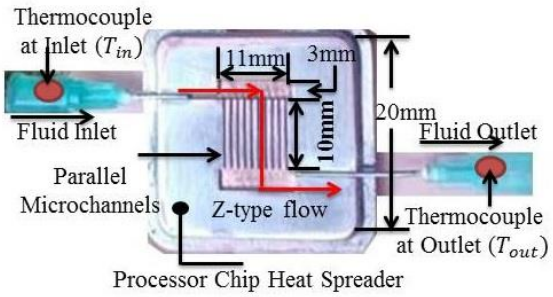

(b)

Fig. 1 Microchannel heat sink (a) Heat spreader of Intel® Core™ i7 processor chip (b) Z-type flow arrangement in multi-microchannel test section with inlet/outlet ports and manifolds

2.2 Experimental Set-up

All ten parallel microchannels had a square cross section. They were receiving coolant from the inlet manifold having a rectangular cross section. Needles having inner diameter of 750µm were attached at the inlet and outlet ports to receive and discharge coolant, respectively. The coolant flow was pumped to the inlet manifold via needle. Two thermocouples were attached at the end of needles to observe inlet and outlet temperature of the coolant. A multipoint digital temperature indicator configured with k-type thermocouples (Type: k-type, Material: Chromel Alumel, Range: 0-1000°C) was utilised. The size of the thermocouple measuring element used was 500µm. The size of inlet and outlet needles was 750µm. To avoid possible blockage of the coolant in the path, the circular needles were fixed with a larger diameter part at the end (injection syringe needle). Thermocouple measuring element has been inserted into these parts, to measure inlet and outlet temperature of the coolant. There was no direct connection between circular ports and square microchannels, as shown in Fig. 1(b). A peristaltic mini pump (Model: DC 12VD2, Fluid supply: 5-85 ml/min) was employed to provide coolant from the fluid reservoir to the storage tank via the MCHS. A container with a weighing meter and a timer was used to determine the volume flow rate of the working fluid. The top surface of the test section, i.e. MCHS was covered by attaching clear hammered glassware using glue of Permabond instant adhesive 825, Pick +200°C, having low viscosity cyanoacrylate with high temperature resistance. It was

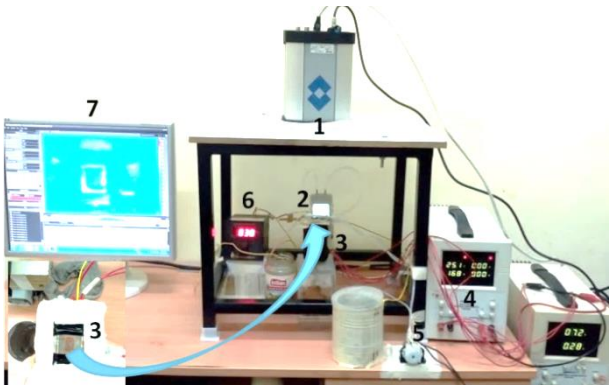

1. Infrared camera 2. Pressure sensors 3. MSHS with cartridge heater assembly 4. Power source 5. Pumping device 6. Temperature sensors 7. Arrangement for Image acquiring

Fig. 2 Pictorial view of experimental set-up

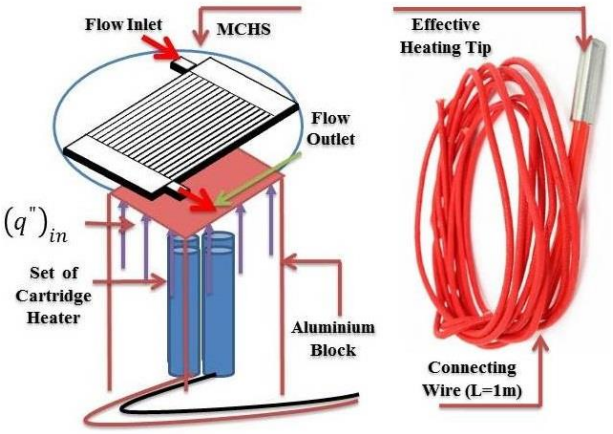

Fig. 3 Cartridge heater assembly

helpful to prevent the leakage of working fluid from the top side of the MCHS. Figure 2 depicts a visual representation of the experimental set-up. To apply thermal load to the heat spreader, four number of cartridge heaters were attached at the bottom surface. The cartridge heater assembly with 4 sets of 304 cylindrical stainless steel (24V, 40W) cartridge heaters is shown in Fig. 3. This way, almost constant heat flux of $95\,W/cm^2$ was achieved equivalent to the thermal design power (TDP) of the Intel® Core™ i7 processor (95W) applied to the area of $1cm^2$. Except for the top portion, all remaining surfaces were fully insulated with $20mm$ thick glass wool to prevent heat loss. The current of the heating unit assembly was managed by a compact digital dual display power supply of $30V - 3A$.

A FLIR thermal infrared camera (Model: SC4000, Spectral range: $3-5\mu m$ pixels: 320×256, pixel size: $30\mu m \times 30\mu m$ resolution: $14bit$, and max. frame rate: $48.5kHz$) was employed to acquire the temperature of microchannel surface in the form of thermo-graphic imaging captured from the top surfaces of the MCHS test section using research IR software (64bit and version: 4.40.6.24) coupled with desktop PC (Intel® Core™ 2 CPU 6600@2.40 GHz 64-bit Operating system Window 7, RAM: 4GB, and ROM: 325GB). IR camera was vertically mounted on the MCHS. For holding of the thermal IR camera, the specific design (top: size $14" \times 14"$) table was fabricated with a central square slot ($4" \times 4"$) to provide direct access of the MCHS channel surface for thermal image capture, as shown in Fig. 2.

The electronic manometer (Model: HT-1895, pressure span: 0.51MPa, resolution: 0.001MPa, and precision: 0.3% full scale output) was utilized to monitor the pressure difference across MCHS. For better understanding, all the arrangements of measuring instruments, heating source, power supply, fluid driven system, and thermal image capturing unit are also shown in Fig. 4.

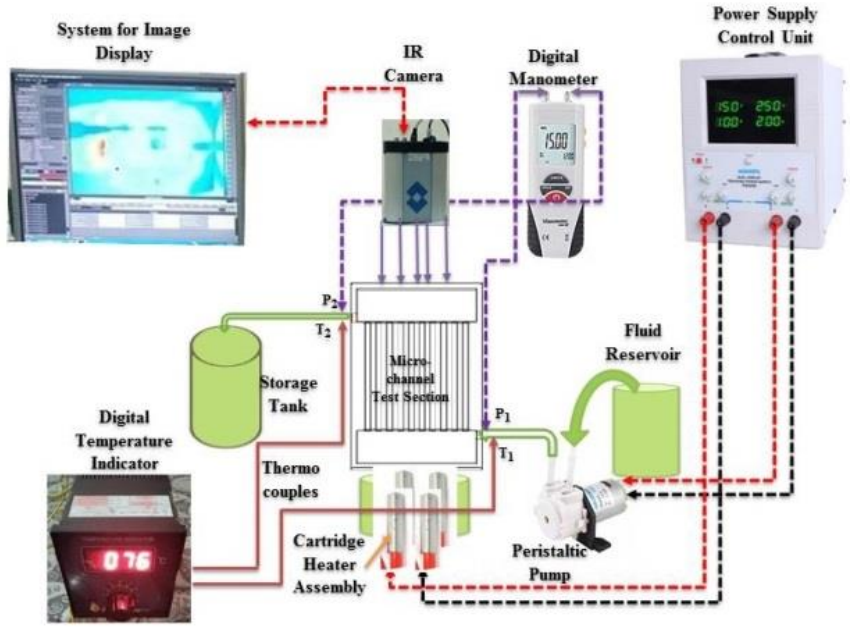

Fig. 4 Schematic diagram of Experimental test setup

2.3 Uncertainty Estimation

To check the reliability and accuracy of the experimental system, the error propagation method (Andraos, 1996) was adopted to estimate the uncertainty of dependent variables. The maximum measured parameter uncertainty as heat input ($\pm 3\%$), thermal conductivity ($+5\%$), dynamic viscosity (-5%), pressure drop ($\pm 2.5\%$), and temperature ($\pm 5\%$) was calculated. The same has been performed to calculate the uncertainty for estimated parameters such as Reynolds number ($\pm 3.8\%$), friction factor ($\pm 4.0\%$), convective heat transfer coefficient ($\pm 6.5\%$), and average Nusselt number ($\pm 8\%$).

2.4 Experimental Procedure

The fluid reservoir was first filled with DW as coolant in a predetermined quantity. By altering the operational voltage of an adjustable velocity peristaltic pump, the required volumetric flow level was achieved. The coolant was pumped from the fluid reservoir to the storage tank via MCHS using a peristaltic mini pump. The coolant enters the MCHS through the inlet intake manifold and distributed to all the ten microchannels, according to Z-type flow configuration. The power system voltage regulator was adjusted to achieve a constant heat flux of 95W/cm^2. Convective heat transfer between coolant and MCHS surface takes place. After reaching steady-state conditions, the fluid temperatures at the inlet and outlet were measured. To avoid practical difficulty of MCHS wall surface temperature measurement by installing thermocouples at the bottom of the heat spreader ($250\mu m$ thick), thermal IR camera was used to record temperatures at 8 points (T_1 to T_8) located approximately in between microchannel numbers 1, 3, 5, 8, and 10 and average surface temperature was obtained (Fig. 5). The distribution pattern of 8 points was considered spread over the full heat sink area with symmetry from the first to the last microchannel. To ensure the reproducibility of the volume flow per unit time, MCHS surface temperatures and pressure distribution across MCHS were tested thrice. An initial series of experiments were carried out using DW at Reynolds numbers ranging from 1000 to 1800. The experiments were further carried out using nanofluids with different nanoparticle concentrations with the same range of Reynolds numbers.

Detailed descriptions of range and flow variables are given in Table1.

2.5 Experimental Data Reduction

The cartridge heater was utilised to supply the heat flux the bottom of the MCHS surface obtained using Equation 1.

$$q^{"} = Q/A_s \tag{1}$$

Heat transfer by coolant in parallel microchannels was estimated from the temperature of MCHS inlet port and outlet port by energy balance, using Equation 2.

$$Q = \dot{m}c_p(T_{out} - T_{in}) \tag{2}$$

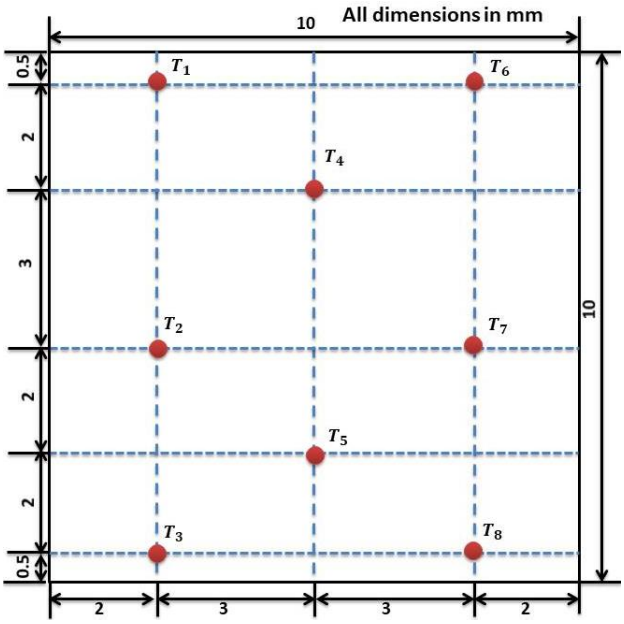

Fig. 5 Schematic for MCHS channel wall surface temperature measurement

Table 1 Range of thermal and flow variables

Variables	Range
Reynolds number, *(Re)*	$1000 - 1800$
Nano-particle concentration	$1vol.\% - 3vol.\%$
Flow arrangement	Z-Type
Wall Heat flux $(q^{"})$	$95\ \mathrm{W/cm^2}$

where, $\dot{m} = \rho A v_f$, is the mass flow rate in kg/s at the inlet port, c_p is specific heat capacity of coolant in $j/kg - K$ and T_{in} is the inlet temperature and T_{out} is the outlet fluid temperature in K.

The flow Reynolds number (Re) at the flow inlet was defined using Equation 3.

$$Re = \frac{\rho V_f \mathrm{D}}{\mu} \tag{3}$$

where, $v_f = \frac{Re \times \mu}{\rho D}$ is the velocity of fluid in m/s, ρ is the density of fluid in kg/m^3, μ is the dynamic viscosity in $kg/m.s$. and D is the diameter of inlet port needle in m.

The average Nusselt number of MCHS was calculated using Equation 4.

$$Nu_{avg} = \frac{\mathrm{h}_{avg} \times D_h}{k_f} \tag{4}$$

where, k_f represents the thermal conductivity of the flowing fluid at the bulk fluid mean temperature T_m, measured from the inlet and outlet fluid temperatures, and D_h as channel hydraulic diameter.

The average HTC was estimated using Equation 5 (Brighenti et al., 2013; Karimzadehkhouei et al., 2019; Dahiya et al., 2020).

$$h_{avg} = \frac{Q}{A_s(T_s - T_m)} \tag{5}$$

where, A_s is the effective heat surface area in m^2, T_s is the average surface temperature of MCHS (average of T_1 to T_8) measured using thermal IR camera in ℃, and T_m is the mean bulk fluid temperature, estimated from the inlet and outlet fluid temperatures as $(T_{in} + T_{out})/2$ in ℃.

The friction factor (f) that represents the fluid flow performance of MCHS was calculated using Equation 6.

$$f_{exp} = \frac{D_h \Delta P}{0.5 \rho v_f^2 L} \tag{6}$$

where, ΔP is the measured pressure drop across the MCHS and L is the length of microchannels.

2.6 Characterization, Stability and Thermo-Physical Property Measurement

Three-step recommendations were used to choose Al_2O_3/water nanofluids with three different nanoparticle fractions (1-3 vol.%) as heat transfer fluids (Asadi, 2018). $Al_2O_3/water$ nanofluids with different nanoparticle fractions (1-3 vol.%) were prepared employing a two-step technique at the Nano Research Lab in Jamshedpur (JH), India, (Suresh et al., 2011; Ali & Salam, 2020). The solution was shaken vigorously and stirred manually for 10 minutes before being ultrasonicated to break up any probable nanoparticle agglomeration.

For the nanoparticle characterization various techniques were available in the literature as transmission electron microscopy (TEM), x-ray diffraction (XRD) techniques and scanning electron microscopy (SEM). The SEM technique was used to analyze Al_2O_3 nanoparticles by evaluating their particle size and shape (FEI Quanta™ 250, Thermo ScientificQuanta™, USA). A droplet of colloid fluid was dried under the influence of daylight to produce the nanoparticle specimen. The resulting nanoparticle specimen was smashed and subjected to SEM analysis. The findings specify that the shape of aluminium oxide nanoparticles was virtually rounded, but the particles were enlarged according to Fig. 6. Hydrodynamic granular diameter and zeta potential of Al_2O_3/water nanofluid were determined utilizing a consumable foldable capillary cell and a Zetasizer Nano ZS-90. This device operates on the Quasi Elastic Light Scattering, electrophoresis light scattering, and statically dispersion principles. Figure 7(a) depicts the hydrodynamic granular diameter variation based on the strength of the $Al_2O_3/water$ nanofluid. The figure depicts a restricted Gaussian distribution of element dimension, culminating at roughly 486 nm, which is 10 times the baseline nanoparticle dimension.

To evaluate the durability of nanofluids, various approaches were employed, including sedimentation, sedimentation-balance, zeta potential, and spectrum analysis methods. The zeta potential approach was employed in this work to assess dispersibility. The zeta potential of $Al_2O_3/water$ nanofluid was quantified to determine dispersibility. Figure 7(b) depicts the zeta potential distribution of $Al_2O_3/water$ nanofluid. The greatest value of zeta potential indicates the steady suspension of a H_2O-based nanofluid. The findings demonstrated that a maximum level of the zeta potential

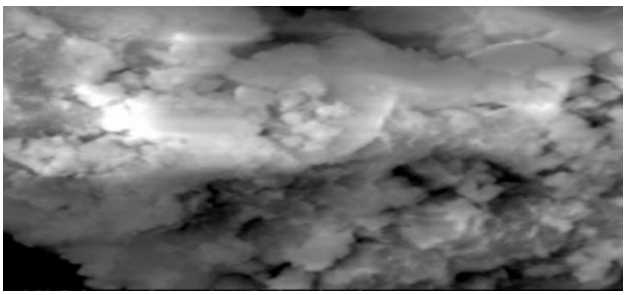

Fig. 6 Nanoparticle characterization using SEM

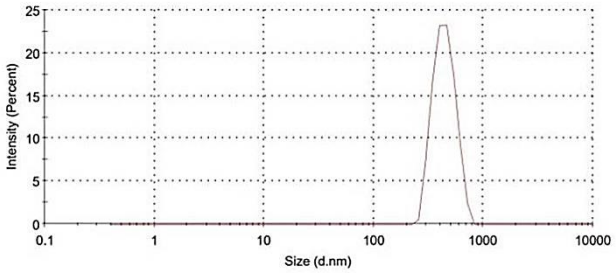

(a) Particle size

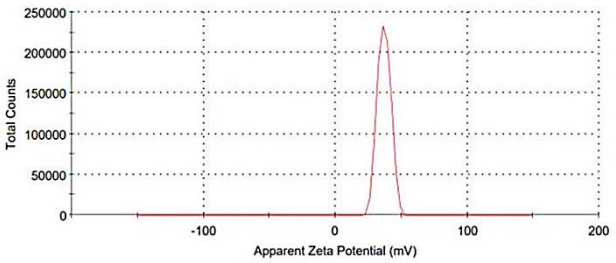

(b) Zeta potential

Fig. 7 Variation of particle size and Zeta potential distribution of Al_2O_3/water nanofluid

of +37 millivolts was reached, showing that nanofluids were stable (Choudhary et al., 2017).

The thermo-physical properties of $Al_2O_3/water$ nanofluid was evaluated using existing models (Krieger & Dougherty, 1959; Prasher et al., 2005, 2006; Chen et al., 2007).

Applying Newton's model, the density of Al_2O_3/water nanofluids was computed using Equation 7 (Yadav et al., 2019).

$$\rho_{nf}(\emptyset, T) = (1 - \emptyset)\rho_{bf}(T) + \emptyset\rho_{np} \tag{7}$$

Similarly, the Pak and Cho model was used to evaluate the specific heat of Al_2O_3/water nanofluids using Equation 8 (Bock Choon Pak, 2013).

$$C_{p,nf}.(\emptyset.T) = \frac{(1 - \emptyset)\rho_{bf}(T)C_{p,bf}(T) + \emptyset\rho_{np}C_{p,np}}{(1 - \emptyset)\rho_{bf}(T) + \emptyset\rho_{np}} \tag{8}$$

The model proposed by Prasher et al. to predict the thermal conductivity of alumina nanoparticles in DW was expressed using Equation 9. (Prasher et al., 2006).

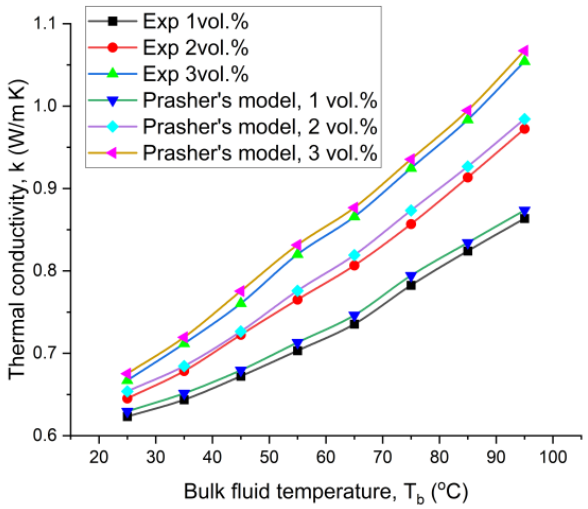

(a) Thermal conductivity

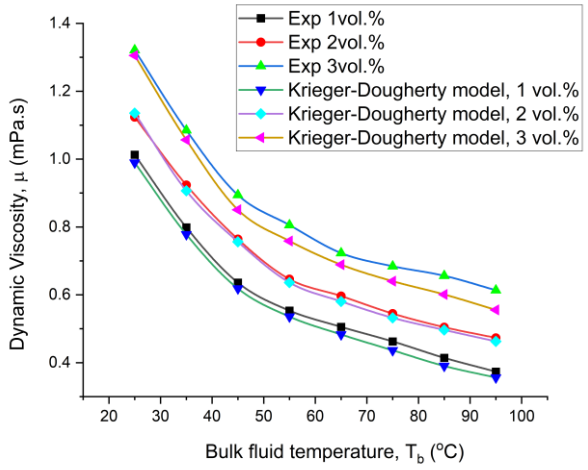

(b) Dynamic viscosity

Fig. 8 Assessment of experimental and anticipated values for Al_2O_3/water nanofluids utilizing known characteristic models

$$\frac{k_{nf}(\emptyset,T)}{k_{bf}(T)} = \left(1 + A.\,Re_B^m Pr_{bf}^{0.333}\emptyset\right) \times \left[\frac{\left[k_{np}(1+2\alpha_B)+2k_m\right]+2\emptyset\left[k_{np}(1-\alpha_B)-k_m\right]}{\left[k_{np}(1+2\alpha_B)+2k_m\right]-\emptyset\left[k_{np}(1-\alpha_B)-k_m\right]}\right] \quad (9)$$

Where, $\alpha_B = \frac{2R_b k_m}{d_{np}}$ and $k_m = k_{bf}\left[1 + \left(1/4\right)Re_{bf}pr_{bf}\right]$

Also, the modified model proposed by Krieger-Dougherty for the estimation of the dynamic viscosity of alumina nanoparticles in DW was used as expressed by Equation 10. (Deepak Selvakumar & Dhinakaran, 2017; Suresh et al., 2011) as

$$\mu_{nf}(\emptyset.T) = \mu_{bf}(T)\left(1 - \frac{\emptyset_a}{\emptyset_{max}}\right)^{-[2.5]\emptyset_{max}} \quad (10)$$

Where, $\emptyset_a$ the vol. concentration of comprehensive nanoparticles is expressed using the Equation 11 as:

$$\emptyset_a = \emptyset\left(\frac{a_a}{a}\right)^{3-D_f} \quad (11)$$

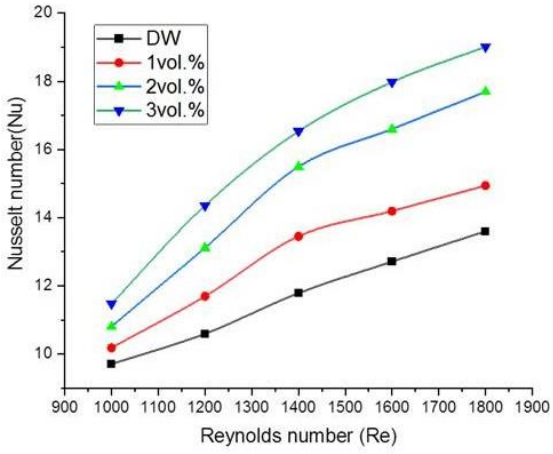

Fig. 9 Nusselt number (Nu) at different concentration of nanoparticles and Re number

Here, $\emptyset_{max}$ is the highest particle packing segment at which flow occurs and was approximately considered as 60.5×10^{-2} and D_f is the fractal dimension and was considered as 2.499 (Krieger & Dougherty, 1959).

Figures 8(a) and 8(b) provide an overview of test findings for thermal conductivity and dynamic viscosity with projected values from existing property models for $Al_2O_3/water$ nanofluid at varied nanoparticle levels (Ø=1-3vol.%). Findings show that the thermal conductivity of $Al_2O_3/water$ nanofluid was matching well with the existing characteristic model of Prasher et al. within +5 % under prediction, while that of dynamic viscosity was matching well with the existing characteristic model of Krieger et al. within -5 % over prediction.

3. RESULTS AND DISCUSSION

The measured data was used to obtain Nusselt number, convective heat transfer coefficient, and friction factor of $DW\ and\ Al_2O_3/water$ nanofluids to observe the consequences of various nano-particle concentrations over DW towards better heat transfer. Experimental results were also observed from thermal imaging to obtain the changes in the maximum MCHS wall surface temperature with increasing Reynolds number. Friction factor was calculated to analyze the pumping power cost over the increase heat transfer rate. Furthermore, the Nusselt number and friction factor correlations for $Al_2O_3/water$ nanofluid were developed and checked for their prediction accuracy.

3.1 Effect of Nanoparticle Concentration on Nusselt Number

Figure 9 depicts the variations among the Nusselt number and Reynolds numbers for $Al_2O_3/water$ nanofluids with 3 distinct volume fractions (1-3vol.%) considering fixed heat flux applied to bottom wall of MCHS. It was found that the Nusselt number rises with rising Reynolds number for all the coolants. This obvious trend is attributed to the increased flow velocity. A notable improvement in the Nusselt number of 39% was

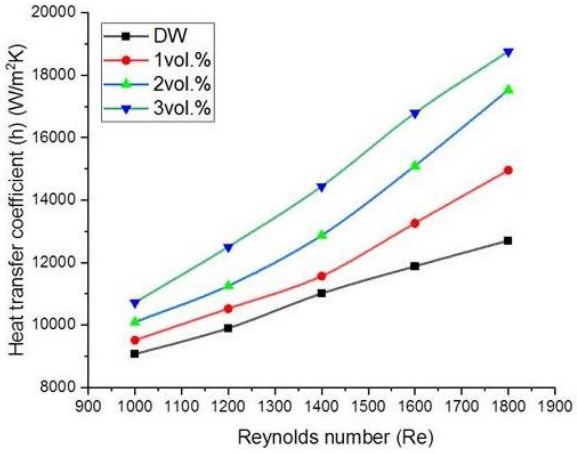

Fig. 10 Heat transfer coefficient at different nanoparticle concentration and Re number

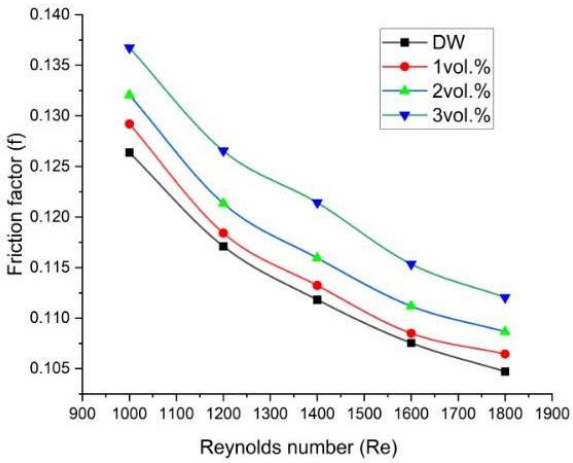

Fig. 11 Changes in Friction factor with Reynolds number

seen upon increasing the percentage of nanoparticles from 1 vol.% to 2 vol.% with Reynolds number ranging from 1500 to 1800; as compared to that of 1vol.% and DW where rate of increase can be seen decreasing beyond Reynolds number of 1400. This was owing to a significant improvement in fluid flow behaviour added by higher thermal conductivity as a result of nanoparticle concentration. Further increasing the nanoparticle concentration from 2vol.% to 3vol.% although brings increase in Nusselt number but not at the same rate.

3.2 Effect of Particle Concentration of Nanofluid on Convective Heat Transfer Coefficient

Figure 10 depicts the Reynolds number vs. convective heat transfer coefficient variation at varied nanoparticle quantities. In all experiments, the heat transfer coefficient upsurges by increased Reynolds number. It was evident that there was a direct correlation between the heat transfer coefficient and Reynolds number. As the Reynolds number increases, the slope also increases. The increase in heat transfer coefficient was up to 41% for a higher Reynolds number, but it was about 18% for a lower Reynolds number of 1000. Again, a distinctive rate of increase can be seen with 2vol.% particle concentration.

3.3 Effect of Nanoparticle Concentration on Friction Factor

To keep the pumping power cost of microchannel cooling technology to a minimum, lower friction factor is targeted. Figure 11 depicts the variability of the friction factor with Reynolds number (1000-1800) for 3 distinct particle concentrations (1-3 vol.%). The findings indicate that although the trend was similar with all the fluids, i.e. a drop in friction factor through a rise in Reynolds number, the friction factor was highest with 3 vol.% of nanoparticles. The reason for higher friction factor is directly related to increase in fluid viscosity with increase in nanoparticle concentration. When the number of nanoparticles increases, a discernible rise in the friction factor is found regardless of the Reynolds number. Here again, maximum benefit was obtained with 2 vol.% contributing to only 4.32% increase. Nanofluid with 3 vol.% contributed to 7.31% increase in friction factor together with marginal increase in HTC over 2 vol.%. It can be concluded here that nanofluid with 2 vol.% can be employed for cooling processor chip without much pumping cost.

3.4 Thermal IR Images

During each set of experiments, changes in surface temperature of MCHS wall at various Reynolds numbers (1000-1800) were recorded. Figures 12 (a), (b), (c), and (d) show respective IR images. As can be seen vividly, surface temperatures are decreasing with an increase in Re number, owing to heat transfer enhancement. With DW, At Re=1000, the data show a hot spot with MCHS surface temperature of 92.7°C. The wall surface temperature of MCHS drops with increasing Reynolds number from 1000 to 1800. The maximum surface temperature was about 92.7, 88.2, 80.7, 77.9, and 76.1°C for 1000, 1200, 1400, 1600, and 1800 Reynolds numbers respectively. At Reynolds number of 1800, maximum temperature (hot spot region) was just above critical temperature of 75ºC, indicating vulnerable spot which may trigger chip failure due to overheating. The surface temperatures were different for different nanoparticle concentrations with changing hot spot regions and their temperatures. Each of the nanofluid could bring the maximum surface temperature below the critical value at Reynolds number of 1800, indicating vividly contribution of enhanced thermal conductivity on heat transfer. Finally, with 3vol %, the maximum surface temperature of 86.3, 80, 77, 73.1, and 70.7°C were achieved with Re, a decrease of about 5-6ºC as compared to DW.

3.5 Development of Correlations

Considering experimental data, novel correlations of the average Nusselt number and friction factor have been established for $Al_2O_3/water$ nanofluid with Z-type flow configured heat sink.

For the development of correlations, Minitab statistical software was used, and the following procedure was adopted.

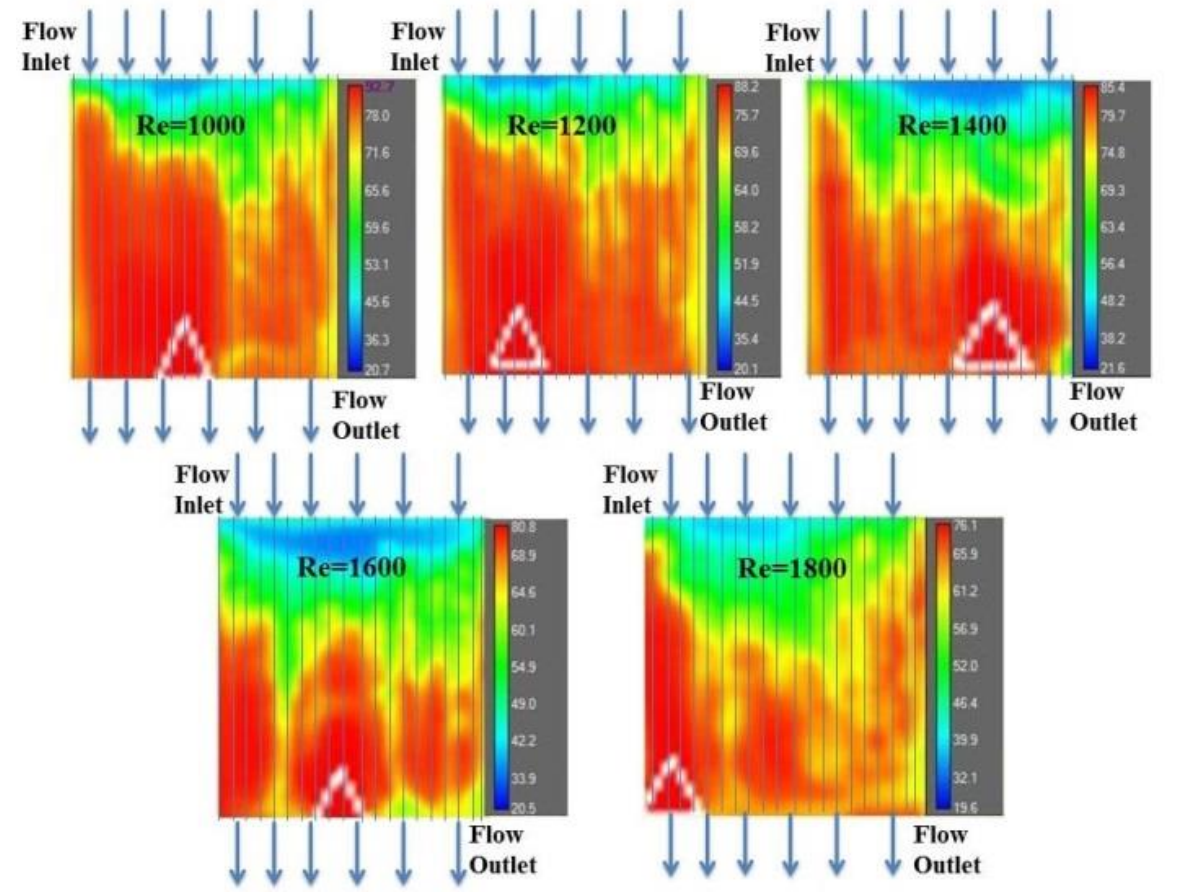
Flow Inlet
Re=1000
Flow Outlet
Flow Inlet
Re=1200
Flow Outlet
Flow Inlet
Re=1400
Flow Outlet
Flow Inlet
Re=1600
Flow Outlet
Flow Inlet
Re=1800
Flow Outlet

(a) DW

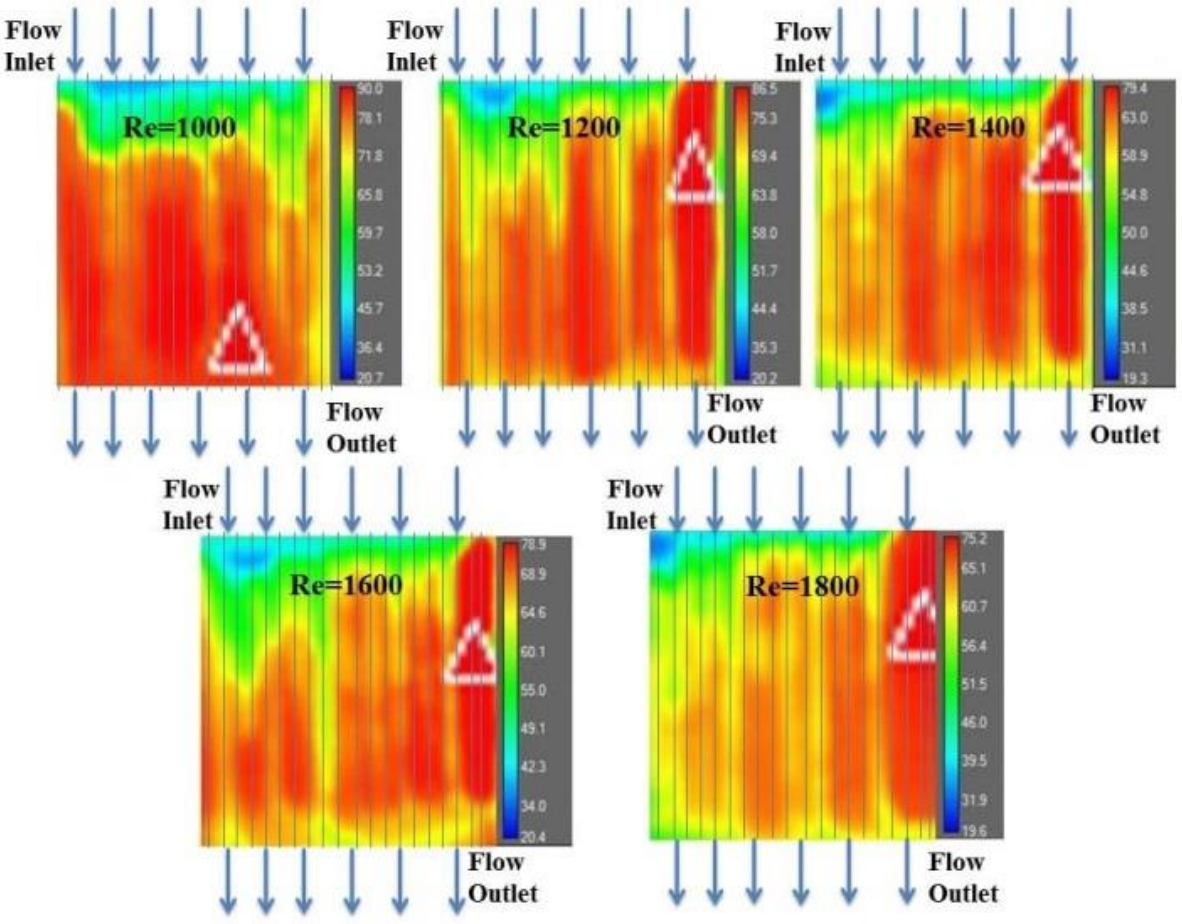
Flow Inlet
Re=1000
Flow Outlet
Flow Inlet
Re=1200
Flow Outlet
Flow Inlet
Re=1400
Flow Outlet
Flow Inlet
Re=1600
Flow Outlet
Flow Inlet
Re=1800
Flow Outlet

(b) 1vol.%

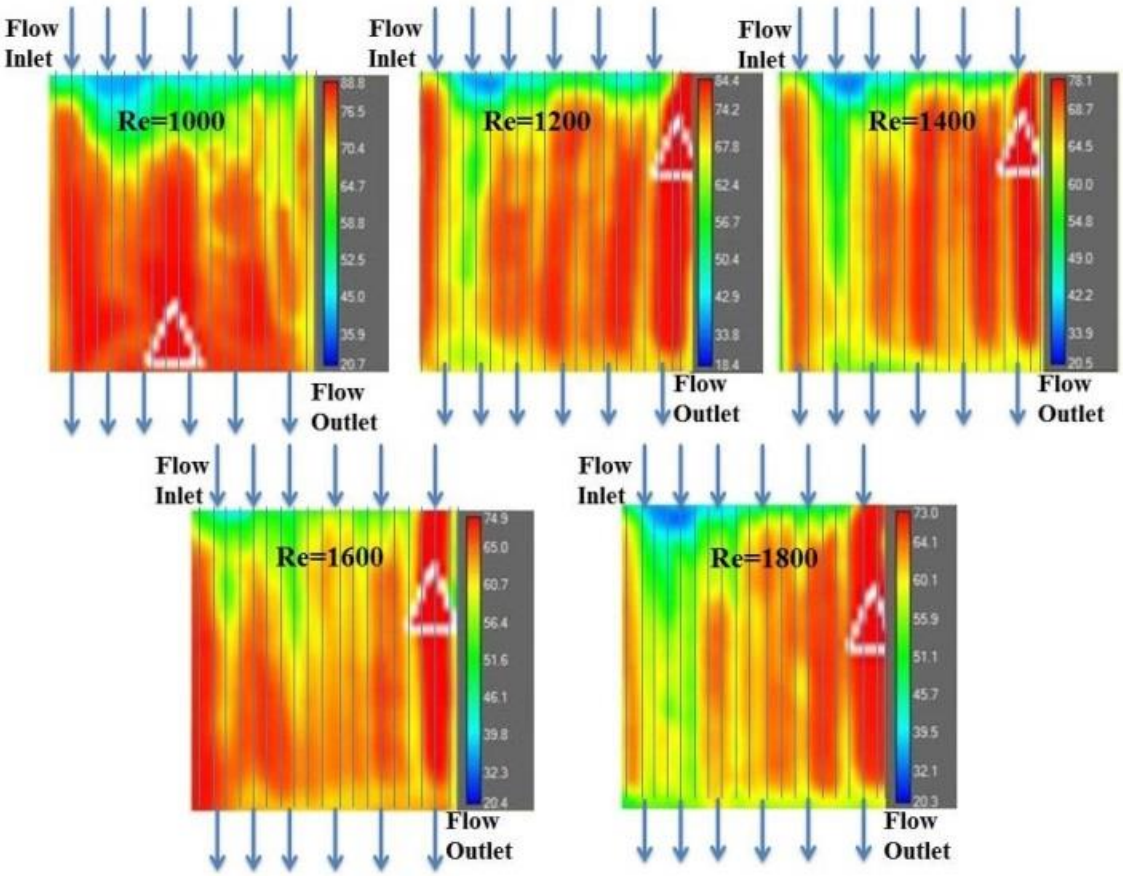

(c) 2 vol.%

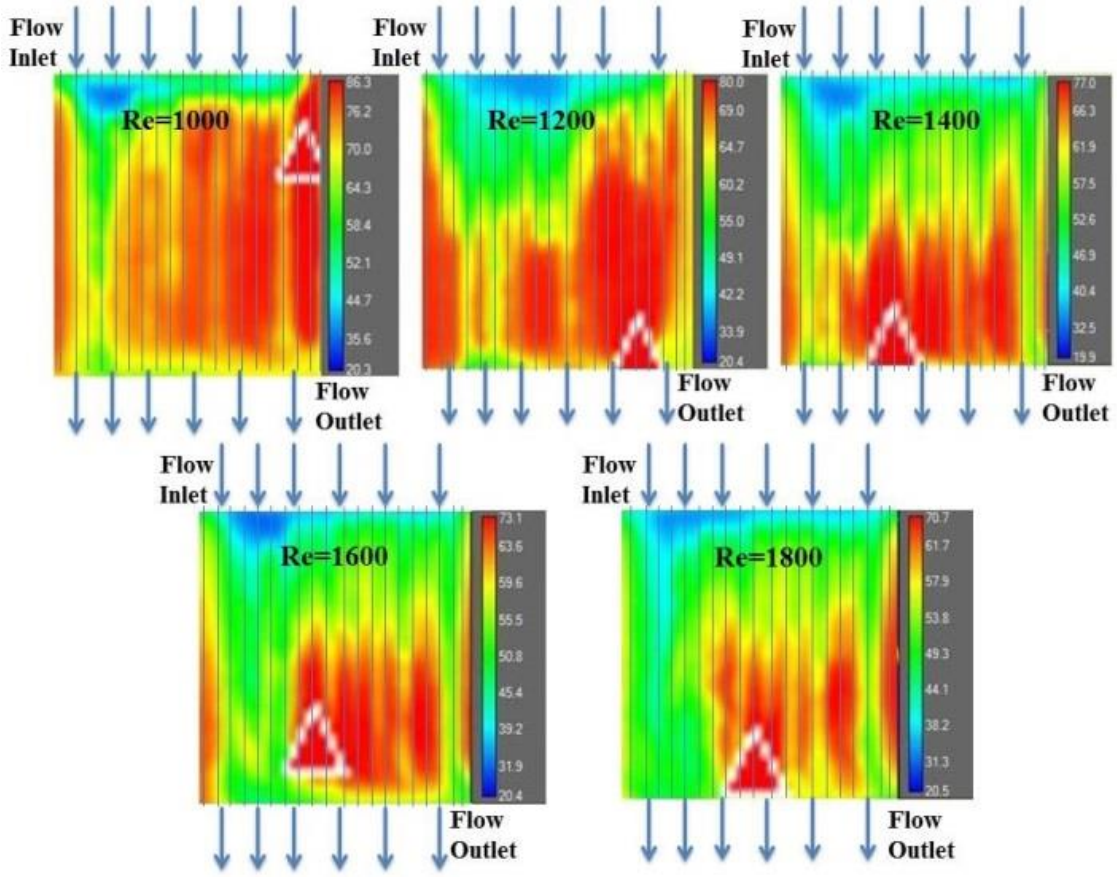

(d) 3 vol.%

Fig. 12 Thermal IR images at four different Reynolds number at fixed wall heat flux

Step-I: The correlation applied to different geometries and flow conditions with the consideration of average Nusselt number as a function of Reynolds number, Prandtl number, and particle concentration of nanofluid was expressed using Equation 12.

$$\mathrm{Nu_{avg}} = \mathrm{k(Re)^a}\left[\frac{\mathrm{L\times N/D_h}}{\mathrm{RePr}}\right]^{\mathrm{b}}(1+\emptyset)^{\mathrm{c}} \quad (12)$$

where, $\left[\frac{\mathrm{L\times N/D_h}}{\mathrm{RePr}}\right]$is the dimensionless thermally developing axial length of MCHS and substituted by $\frac{200}{\mathrm{RePr}}$, k is the empirical constant in the equation, while a, b, and c are the regression coefficients.

Similarly, the correlation used for friction factor for $Al_2O_3/water$ nanofluid was given in Equation. 13:

$$f = k(\mathrm{Re})^{a}\left[\frac{\mathrm{L\times N/D_h}}{Re}\right]^{b}(1+\emptyset)^{c} \quad (13)$$

where, $\left[\frac{\mathrm{L\times N/D_h}}{Re}\right]$ is the dimensionless hydrodynamically developing axial length of MCHS and substituted by $\frac{200}{\mathrm{Re}}$.

Step-II: In this step, the Levenberg Marquardt (Yamashita & Fukushima, 2001) method was used to estimate the values of κ, a, b, and c by solving Equations 12 and 13 as given in Table 2.

Step III: After incorporating all the values of empirical constant and regression coefficients in Equation 12, correlation developed for the average Nusselt number is illustrated by Equation 14:

$$\mathrm{Nu_{avg}} = 0.188(\mathrm{Re})^{0.451}\times\left[\frac{200}{RePr}\right]^{-0.258}\times(1+\emptyset)^{12.75} \quad (14)$$

Similarly, after incorporating all the values of empirical constant and regression coefficients, correlation developed for the friction factor is illustrated by Equation. (15):

$$f = 0.122(\mathrm{Re})^{0.037}\times\left[\frac{200}{Re}\right]^{0.171}\times(1+\emptyset)^{1.67} \quad (15)$$

The proposed correlations for average Nusselt number and friction factor have been compared with the existing correlations available in the literature (Zhang et al., 2013; Manay & Sahin, 2016b; Lodhi et al., 2020), for different Reynolds numbers and nanoparticle concentrations, as shown in Figures 13(a) and 13(b). As can be seen vividly, the data of Nusselt number obtained from Zhang et al. correlations revealed similar trend but with a deviation of about 25% under predicted. Similarly, data obtained from Lodhi et al. and Many et al. also show the same trends but significantly under predicting Nusselt

Table 2: Value of regression coefficients

Constants	κ	a	b	c
Nusselt number	0.188	0.451	−0.258	12.75
Friction factor	0.122	0.037	0.171	1.67

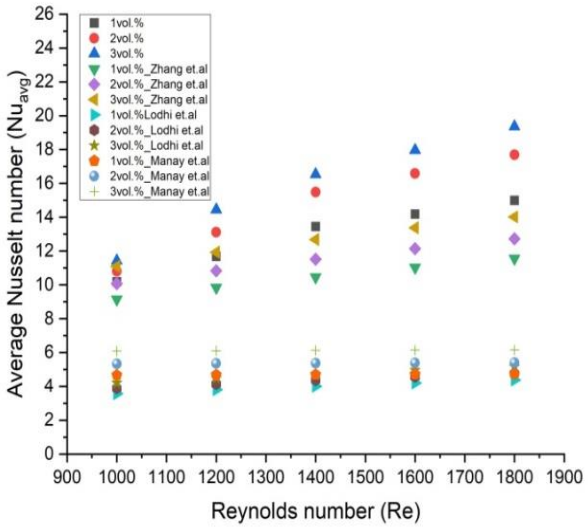

(a) Average Nusselt number

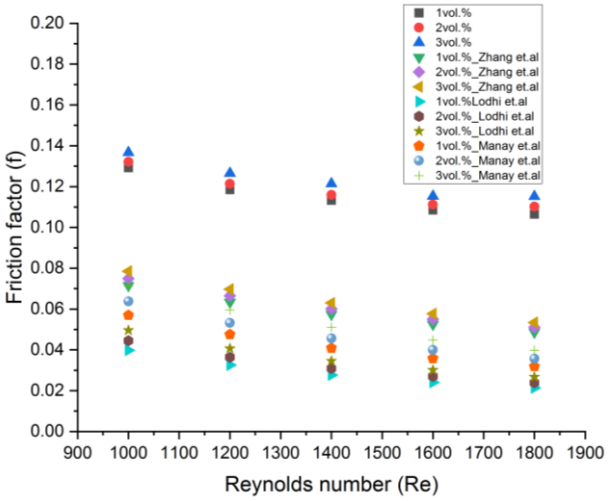

(b) Friction factor

Fig. 13 Illustration of projected data for Al_2O_3/water nanofluid utilizing experimental and available correlation

numbers as shown in Fig. 13(a). The reason for under-prediction is the difference between the flow physics. The proposed correlation is for hydrodynamic as well as thermally developing flow while that of literature is only thermally developing. Figure 13(b) shows a similar trend of friction factor variation with Reynolds number by all the models. The data of friction factor clearly shows a variation of about 30%.

To obtain prediction accuracy of the proposed correlation models, experimental values were compared with that predicted from the models. Points falling along the diagonal indicate accuracy of the prediction. Figure 14(a) shows ±10% accuracy of prediction of the average Nusselt number. The projected friction factor datasets from the suggested correlation clearly lie diagonally, with just ±8% variation from the measured values collected from the present experimental investigation, as shown in Fig. 14(b).

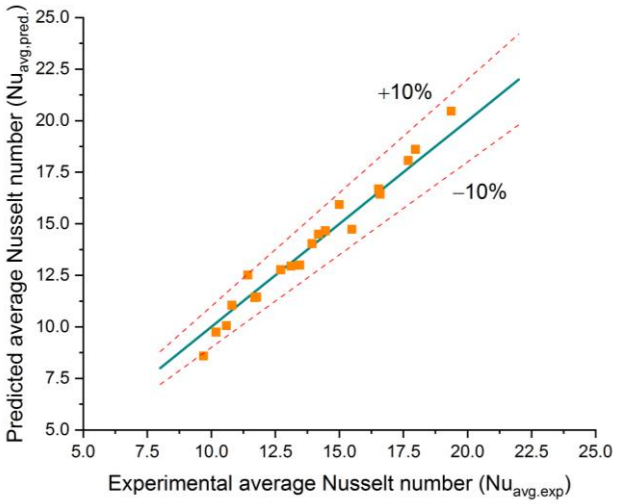

(a) Average Nusselt number

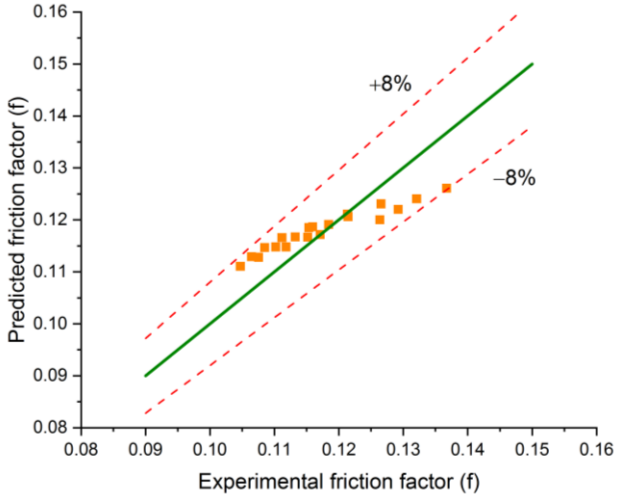

(b) Friction factor

4. CONCLUSION

Experimental investigation was carried out on heat spreader of an actual processor chip by fabricating a multi-MCHS. Constant heat flux of $95 W/cm^2$ was applied to the bottom of the MCHS as thermal load, equivalent to TDP of the Intel® core™ i7 processor chip. Cartridge heaters were used to apply heat flux mimicking the actual processor chip heating.

Initially, the nanofluid was characterized and stability as well as thermo-physical properties were analyzed to measure the heat transfer and flow features of a Z-type flow MCHS. After that, the impact of alumina particle concentration (0-3 vol.%) in DW was analyzed for heat transfer and flow features in microchannels with thermally and hydrodynamically developing laminar flow measured at Reynolds numbers varying from 1000-1800. Furthermore, correlations between the average Nusselt number and friction factor were established. The following conclusions were drawn from the investigation.

1. Advantage of smaller size microchannels have been observed in terms of flow field being hydrodynamically as well as thermally developing.
2. Nanofluid with 2 vol.% can be employed for cooling processor chips without much pumping cost.
3. The increase in average heat transfer coefficient surpasses increase in friction factor. Thus, providing effective cooling without increasing pumping power.
4. The developed correlations for average Nusselt number and friction factor could predict the experimental data within $\pm 10\%$ and $\pm 8\%$, accuracy, respectively. The proposed models can be utilized for prediction of possible chip cooling in industrial applications.
5. Overall, the industrial-grade heat spreader was opted to fabricate the microchannels on the back of its surface and tested for the equivalent heat flux loading as system TDP. It shows that the kind of MCHS proposed can be a possible solution for the electronic processor chip cooling.

ACKNOWLEDGEMENTS

The authors are grateful to IIITDM Jabalpur (MP), for the Research facilities.

CONFLICT OF INTEREST

No conflicts to disclose.

AUTHORS CONTRIBUTION

Devisingh Rawat: Investigation and writing original draft; **M. S. Lodhi:** Conceptualization and methodology; **Tanuja Sheorey:** Supervision writing and editing.

REFERENCES

Ali, A. R. I., & Salam, B. (2020). A review on nanofluid: preparation, stability, thermophysical properties, heat transfer characteristics and application. *SN Applied Sciences*, *2*(10). https://doi.org/10.1007/s42452-020-03427-1

Alihosseini, Y., Zabetian Targhi, M., Heyhat, M. M., & Ghorbani, N. (2020). Effect of a micro heat sink geometric design on thermo-hydraulic performance: A review. *Applied Thermal Engineering*, *170* (September 2019), 114974. https://doi.org/10.1016/j.applthermaleng.2020.114974

Andraos, J. (1996). On the propagation of statistical errors for a function of several variables. *Journal of Chemical Education* 73(2), 150–154. https://doi.org/10.1021/ed073p150

Asadi, A. (2018). A guideline towards easing the decision-making process in selecting an effective nanofluid as a heat transfer fluid. *Energy Conversion and Management*, *175*(August), 1–10.

https://doi.org/10.1016/j.enconman.2018.08.101

Azizi, Z., Alamdari, A., & Malayeri, M. R. (2015). Convective heat transfer of Cu-water nanofluid in a cylindrical microchannel heat sink. *Energy Conversion and Management*, *101*, 515–524. https://doi.org/10.1016/j.enconman.2015.05.073

Azizi, Z., Alamdari, A., & Malayeri, M. R. (2016). Thermal performance and friction factor of a cylindrical microchannel heat sink cooled by Cu-water nanofluid. *Applied Thermal Engineering*, *99*, 970–978. https://doi.org/10.1016/j.applthermaleng.2016.01.140

Behi, M., Shakorian-poor, M., Mirmohammadi, S. A., Behi, H., Rubio, J. I., Nikkam, N., Farzaneh-Gord, M., Gan, Y., & Behnia, M. (2020). Experimental and numerical investigation on hydrothermal performance of nanofluids in micro-tubes. *Energy*, *193*, 116658. https://doi.org/10.1016/j.energy.2019.116658

Bock Choon Pak, Y. I. C. (2013). Hydrodynamic and heat transfer study of dispersed fluids with submicron metallic oxide. *Experimental Heat Transfer : A Journal of , Thermal Energy Transport , Storage , and Conversion*, *January 2013*, 37–41. https://doi.org/10.1080/08916159808946559

Bowers, J., Cao, H., Qiao, G., Li, Q., Zhang, G., Mura, E., & Ding, Y. (2018). Flow and heat transfer behaviour of nanofluids in microchannels. *Progress in Natural Science: Materials International*, *28*(2), 225–234. https://doi.org/10.1016/j.pnsc.2018.03.005

Brighenti, F., Kamaruzaman, N., & Brandner, J. J. (2013). Investigation of self-similar heat sinks for liquid cooled electronics. *Applied Thermal Engineering*, *59*(1–2), 725–732. https://doi.org/10.1016/j.applthermaleng.2013.01.001

Chabi, A. R., Zarrinabadi, S., Peyghambarzadeh, S. M., Hashemabadi, S. H., & Salimi, M. (2017). Local convective heat transfer coefficient and friction factor of CuO/water nanofluid in a microchannel heat sink. *Heat and Mass Transfer/Waerme- Und Stoffuebertragung*, *53*(2), 661–671. https://doi.org/10.1007/s00231-016-1851-0

Chai, L., Xia, G., Zhou, M., Li, J., & Qi, J. (2013). Optimum thermal design of interrupted microchannel heat sink with rectangular ribs in the transverse microchambers. *Applied Thermal Engineering*, 51(1–2), 880–889. https://doi.org/10.1016/j.applthermaleng.2012.10.037

Chen, H., Ding, Y., & Tan, C. (2007). Rheological behaviour of nanofluids. *New Journal of Physics*, *9*. https://doi.org/10.1088/1367-2630/9/10/367

Choudhary, R., Khurana, D., Kumar, A., & Subudhi, S. (2017). Stability analysis of Al2O3/water nanofluids. *Journal of Experimental Nanoscience*, *12*(1), 140–151. https://doi.org/10.1080/17458080.2017.1285445

Dahiya, A., Amer, M., Sajjad, U., Borah, P., Sehgal, S. S., & Singh, H. (2020). An experimental study on microchannel heat sink via different manifold arrangements. *SN Applied Sciences*, *2*(1), 1–11. https://doi.org/10.1007/s42452-019-1784-6

Datta, A., Sanyal, D., Agrawal, A., & Das, A. K. (2019). A review of liquid flow and heat transfer in microchannels with emphasis to electronic cooling. *Sadhana - Academy Proceedings in Engineering Sciences*, 44(12). Springer India. https://doi.org/10.1007/s12046-019-1201-2

Deepak Selvakumar, R., & Dhinakaran, S. (2017). Effective viscosity of nanofluids — A modified Krieger–Dougherty model based on particle size distribution (PSD) analysis. *Journal of Molecular Liquids*, *225*, 20–27. https://doi.org/10.1016/j.molliq.2016.10.137

Herwig, H. (2002). Flow and heat transfer in micro systems: Is everything different or just smaller? *ZAMM Zeitschrift Fur Angewandte Mathematik Und Mechanik*, *82*(9), 579–586. https://doi.org/10.1002/1521-4001(200209)82:9<579::AID-ZAMM579>3.0.CO;2-V

Kandlikar, S. G., & Grande, W. J. (2003). Evolution of microchannel flow passages-thermohydraulic performance and fabrication technology. *Heat Transfer Engineering*, *24*(1), 3–17. https://doi.org/10.1080/01457630304040

Karimzadehkhouei, M., Sadaghiani, A. K., Motezakker, A. R., Akgönül, S., Ozbey, A., Şendur, K., Mengüç, M. P., & Koşar, A. (2019). Experimental and numerical investigation of inlet temperature effect on convective heat transfer of γ-Al2O3/Water nanofluid flows in microtubes. *Heat Transfer Engineering*, *40*(9–10), 738–752. https://doi.org/10.1080/01457632.2018.1442305

Krieger, I. M., & Dougherty, T. J. (1959). A Mechanism for non-newtonian flow in suspensions of rigid spheres. *Transactions of the Society of Rheology*, *3*(1), 137–152. https://doi.org/10.1122/1.548848

Kumaraguruparan, G., Kumaran, R. M., Sornakumar, T., & Sundararajan, T. (2011). A numerical and experimental investigation of flow maldistribution in a micro-channel heat sink. *International Communications in Heat and Mass Transfer*, *38*(10), 1349–1353. https://doi.org/10.1016/j.icheatmasstransfer.2011.08.020

Lodhi, M. S., Sheorey, T., & Dutta, G. (2020). Single-phase fluid flow and heat transfer characteristics of nanofluid in a circular microchannel: Development of flow and heat transfer correlations. *Proceedings of the Institution of Mechanical Engineers, Part C: Journal of Mechanical Engineering Science*, *234*(18), 3689–3708. https://doi.org/10.1177/0954406220916537

Manay, E., & Sahin, B. (2016a). The effect of microchannel height on performance of nanofluids. *International Journal of Heat and Mass Transfer*, *95*, 307–320.

https://doi.org/10.1016/j.ijheatmasstransfer.2015.12.015

Manay, E., & Sahin, B. (2016b). The effect of microchannel height on performance of nanofluids. *International Journal of Heat and Mass Transfer*, *95*, 307–320. https://doi.org/10.1016/j.ijheatmasstransfer.2015.12.015

Manay, E., & Sahin, B. (2017). Heat transfer and pressure drop of nanofluids in a microchannel heat sink. *Heat Transfer Engineering*, *38*(5), 510–522. https://doi.org/10.1080/10407782.2016.1195162

Mohammed Adham, A., Mohd-Ghazali, N., & Ahmad, R. (2013). Thermal and hydrodynamic analysis of microchannel heat sinks: A review. *Renewable and Sustainable Energy Reviews*, *21*, 614–622. https://doi.org/10.1016/j.rser.2013.01.022

Morini, G. L. (2004). Single-phase convective heat transfer in microchannels: A review of experimental results. *International Journal of Thermal Sciences*, *43*(7), 631–651. https://doi.org/10.1016/j.ijthermalsci.2004.01.003

Nikkhah, V., & Nakhjavani, S. (2019). Thermal performance of a micro heat exchanger (MHE) working with zirconia-based nanofluids for industrial cooling. *International Journal of Industrial Chemistry*, *10*(2), 193–204. https://doi.org/10.1007/s40090-019-0183-6

Peng, X. F., & Peterson, G. P. (1996). Convective heat transfer and flow friction for water flow in microchannel structures. *International Journal of Heat and Mass Transfer*, *39*(12), 2599–2608. https://doi.org/10.1016/0017-9310(95)00327-4

Peyghambarzadeh, S. M., Hashemabadi, S. H., Chabi, A. R., & Salimi, M. (2014). Performance of water based CuO and Al2O3 nanofluids in a Cu-Be alloy heat sink with rectangular microchannels. *Energy Conversion and Management*, *86*, 28–38. https://doi.org/10.1016/j.enconman.2014.05.013

Prasher, R., Bhattacharya, P., & Phelan, P. E. (2005). Thermal conductivity of nanoscale colloidal solutions (nanofluids). *Physical Review Letters*, *94*(2), 3–6. https://doi.org/10.1103/PhysRevLett.94.025901

Prasher, R., Bhattacharya, P., & Phelan, P. E. (2006). Brownian-motion-based convective-conductive model for the effective thermal conductivity of nanofluids. *Journal of Heat Transfer*, *128*(6), 588–595. https://doi.org/10.1115/1.2188509

Ramesh, K. N., Sharma, T. K., & Rao, G. A. P. (2021). Latest advancements in heat transfer enhancement in the micro-channel heat sinks: a review. *Archives of Computational Methods in Engineering*, *28*, 3135-3165. https://doi.org/10.1007/s11831-020-09495-1

Roday, A. P., & Jensen, M. K. (2009). A review of the critical heat flux condition in mini-and microchannels. *Journal of Mechanical Science and Technology*, *23*(9), 2529–2547. https://doi.org/10.1007/s12206-009-0711-y

Rostami, A. A., Mujumdar, A. S., & Saniei, N. (2002). Flow and heat transfer for gas flowing in microchannels: A review. *Heat and Mass Transfer/Waerme- Und Stoffuebertragung*, *38*(4–5), 359–367. https://doi.org/10.1007/s002310100247

Smakulski, P., & Pietrowicz, S. (2016). A review of the capabilities of high heat flux removal by porous materials, microchannels and spray cooling techniques. *Applied Thermal Engineering*, *104*, 636–646. https://doi.org/10.1016/j.applthermaleng.2016.05.096

Suresh, S., Venkitaraj, K. P., Selvakumar, P., & Chandrasekar, M. (2011). Synthesis of Al2O3-Cu/water hybrid nanofluids using two step method and its thermo physical properties. *Colloids and Surfaces A: Physicochemical and Engineering Aspects*, *388*(1–3), 41–48. https://doi.org/10.1016/j.colsurfa.2011.08.005

Tuckerman D. B. & Pease, R. F. W. (1981). High-Performance Heat Sinking for VLSI. *IEEE Electron Device Letters*, *2*(5), 126–129. https://doi.org/10.1177/0164027595174002

Vijayalakshmi, K., Anoop, K. B., Patel, H. E., Harikrishna, P. V., Sundararajan, T., & Das, S. K. (2009). Effects of compressibility and transition to turbulence on flow through microchannels. *International Journal of Heat and Mass Transfer*, *52*(9–10), 2196–2204. https://doi.org/10.1016/j.ijheatmasstransfer.2008.07.056

Xu, B., Ooi, K. T., Wong, N. T., & Choi, W. K. (2000). Experimental investigation of flow friction for liquid flow in microchannels. *International Communications in Heat and Mass Transfer*, *27*(8), 1165–1176. https://doi.org/10.1016/S0735-1933(00)00203-7

Yadav, V., Kumar, R., & Narain, A. (2019). Mitigation of flow maldistribution in parallel microchannel heat sink. *IEEE Transactions on Components, Packaging and Manufacturing Technology*, *9*(2), 247–261. https://doi.org/10.1109/TCPMT.2018.2851543

Yamashita, N., & Fukushima, M. (2001). *On the rate of convergence of the levenberg-marquardt method*. In: Alefeld, G., Chen, X. (Eds) Topics in Numerical Analysis. Computing Supplementa, vol 15. Springer, Vienna. https://doi.org/10.1007/978-3-7091-6217-0_18

Zhang, H., Shao, S., Xu, H., & Tian, C. (2013). Heat transfer and flow features of Al2O3-water nanofluids flowing through a circular microchannel - Experimental results and correlations. *Applied Thermal Engineering*, *61*(2), 86–92. https://doi.org/10.1016/j.applthermaleng.2013.07.026